Surface structure and equilibrium particle shape of the $LiMn_2O_4$ spinel from first-principles calculations

Altaf Karim, Sonia Fosse, and Kristin A. Persson
Environmental Energy Technology Division, Lawrence Berkeley National Laboratory, Berkeley, California 94720, USA
(Received 28 November 2012; published 26 February 2013)

First-principles density functional calculations were used to calculate surface properties of the $LiMn_2O_4$ spinel. The calculations were benchmarked to obtain the correct semiconducting, Jahn-Teller distorted electronic ground state of bulk $LiMn_2O_4$ and, using the same parameters, the predominant low-index polar surface facets (100), (110), and (111) were calculated to study their structure and stability. Following an investigation of possible surface terminations as well as surface layer reconstructions we find that the (111) LMO surface stabilizes through a targeted site exchange of the undercoordinated surface Mn cations with fully coordinated tetrahedral subsurface Li cations, effectively creating a partial inverse spinel arrangement at the surface. This reconstruction renders the (111) facet the most stable among the investigated facets. The equilibrium (Wulff) shape of a $LiMn_2O_4$ particle was constructed and exhibits a cubo-octahedral shape with predominant (1 1 1) facets, in agreement with common experimental findings for the spinel structure.

DOI: 10.1103/PhysRevB.87.075322 PACS number(s): 68.35.B−, 68.47.Gh

I. INTRODUCTION

The lithium manganese spinel $LiMn_2O_4$ (LMO) is a promising cathode material for rechargeable Li-ion battery applications[1,2] due to its performance, low cost, and nontoxicity.[3–6] LMO exhibits a cubic spinel structure around or above 290 K,[3,4] is isostructural with $MgAl_2O_4$, and in its discharged state the manganese ions are equally divided between the 3+ and 4+ oxidation states. However, the material exhibits degradation with extended cycling. For example, it is well documented that the LMO exhibits capacity fade,[7,8] possibly related to Mn^{3+} dissolution in the organic electrolyte,[9–12] a process that is aggravated at elevated temperatures.[11] The capacity fade could also be due to the loss of crystallinity during cycling due to formation of oxygen deficiencies, Jahn-Teller (JT) distortion, etc.[13–15] To increase our knowledge about the possible degradation mechanisms and subsequently attempt to modify and improve the performance of this material, it is essential to understand the reactions taking place on the electrode-electrolyte interface, which in turn depends on stability, structure, and composition of the reconstructed surface facets of the material.

The LMO bulk system and its surface structure have been widely studied using both computational and experimental techniques (see, e.g., Refs. 16–21 and references therein). Transmission electron microscope (TEM) images confirm the formation of a solid electrolyte interface (SEI) layer on both the (111) and (110) surfaces of LMO as well as Mn dissolution from the (110) surface.[3–8] LMO surfaces from powder synthesized by solid-state reaction were studied by Huang *et al.*[15] and Takada *et al.*[16] using TEM/SEM techniques. The (111) facet plane was found to be predominant in the LMO crystallites, and remained so on further annealing, which lead to cubo-octahedral crystal morphologies. Molten salt synthesis can result in platelet LMO single crystals, which will grow to cubo-octahedrons with heating time and temperature[22] and while hydrothermal synthesis methods offer significant control of particle shape and size, the (111) surface facet is found to be prevalent under most conditions.[23] First-principles calculations have been used to study the bulk phase transformations as a function of lithiation,[16] Li mobility,[18] and recently extended to the surface properties (see Ouyang *et al.*[20] and Benedek *et al.*[21]). Ouyang *et al.*[20] presented results based on a careful benchmarking of the bulk electronic structure to obtain the correct antiferromagnetic (AF), semiconducting, JT distorted ground state of LMO[19] but limited the surface investigation to the (001) surface facet. Benedek *et al.*[21] carried out an extensive study of all low-index LMO surface terminations for the (100), (110), as well as the (111) facets. A ferromagnetic (FM) arrangement of the Mn ions was employed and molecular dynamics (MD) simulations were utilized to explore the phase space of possible surface reconstructions. However, while experiments show the (111) surface to be the dominant surface facet in LMO, as in most spinels,[24] Benedek *et al.* found, surprisingly, the (100) surface facet to be the most stable from their computations. In view of the importance of the LMO system as a Li-ion cathode material and the proposed connection between the LMO surface stability and its relevance for understanding and improving the performance of the material, we believe it is motivated to revisit the LMO surface structure and stability from a first-principles computational perspective.

To elucidate the chemistry and reactivity of the Mn spinel surfaces, in this work, we undertake an examination of the surface stability, and the resulting equilibrium LMO particle morphology. We first benchmark our methodology by obtaining the correct semiconducting electronic ground state of the LMO bulk material, similarly to the work of Ouyang *et al.*[19] After optimization of the bulk magnetic and electronic state we calculate the low-index (100), (110) and (111) surface energies utilizing multiple terminations and determine the stable, reconstructed surfaces of LMO. Finally, using a minimization of the total surface energy, we predict the equilibrium shape of $LiMn_2O_4$ particles.

II. COMPUTATIONAL METHODOLOGY

All calculations are performed using the generalized gradient approximation (GGA and GGA + U)[25–28] to the

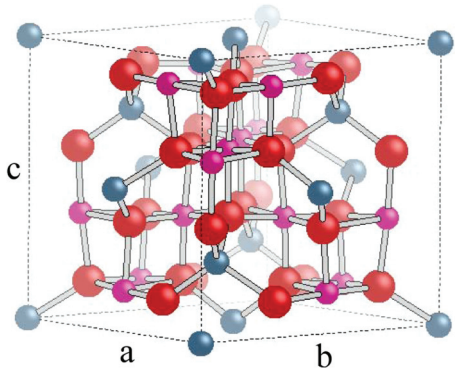

FIG. 1. (Color online) The unit cell of the $LiMn_2O_4$ cubic spinel structure indicating the positions of the Li (blue), the Mn (magenta) and O (red) atomic species.

electron exchange-correlation function within the density functional theory (DFT). The projected augmented wave[29] (PAW) method is used, as it is implemented in the Vienna *ab initio* simulation package (VASP).[30,31] A conventional orthorhombic cell containing eight formula units of $LiMn_2O_4$ was used for the bulk calculations (see Fig. 1). We used an energy cutoff of 550 eV and an $8 \times 8 \times 8$ k-point sampling of the Monkhorst-Pack[32] scheme, which ensured a total energy convergence of the system within 5 meV per atomic unit. The U value for Mn compounds found in the literature varies from 4 to 5 eV.[33–36] In our work, we have chosen a U value of 5 eV after benchmarking to obtain the correct electronic and magnetic state of bulk LMO.

The same parameters were used to calculate the energies and potentials for the different surface facets of the $LiMn_2O_4$ spinel. The unrelaxed structures of (100), (110), and (111) surfaces were extracted from the fully relaxed bulk spinel structure. While performing the surface relaxation calculations we adopted the criterion of Tasker.[37] According to the Tasker criterion, the (100), (110), and (111) surfaces all fall in the category of Type III[38] in which the bare surface has a net polar charge. These surfaces require a redistribution or compensation of charges, such as additional Li ions or oxygen vacancies, on opposite surfaces of the slab, which can be accompanied by a significant rearrangement of the surface atoms (reconstruction). We implemented the slab technique by periodically repeating an infinite number of layers separated by vacuum layers along the surface normal. Both the thickness of vacuum and slab were varied to ensure energy convergence in the given directions. The necessary vacuum thickness, which sufficed to remove interaction between the slabs layers was found to be 8 Å and slabs of 8 layers thickness were chosen in which the four middle layer atoms are fixed and the two top and two bottom layers are allowed to relax during the calculations. A force convergence criterion of 0.02 eV/Å was utilized for the surface relaxations. As the surface index does not specify where to cleave the surface, several possible atomic terminations (Li, Mn, and O) are possible. When possible, we investigated Li, Mn/O as well as Li/Mn/O terminations. The slab volume as well as the internal structural parameters were relaxed, although checks with fixed-volume slab calculations resulted in very similar *relative* surface energies for the different facets.

TABLE I. Calculated and experimental lattice parameters, a, b, and c for $LiMn_2O_4$ bulk spinel.

$LiMn_2O_4$	Exp[46]	GGA	GGA + U	GGA + U + AF
a	8.20 Å	8.09 Å	8.43 Å	8.27 Å
b	8.25 Å	8.09 Å	8.43 Å	8.27 Å
c	8.28 Å	8.09 Å	8.43 Å	8.74 Å

To obtain the equilibrium shape of a crystal we applied the method of the Wulff construction,[39] in which the crystal shape is obtained by minimizing the total surface energy. Similar theoretical investigations have been employed successfully to derive the thermodynamic equilibrium shape for olivine $LiFePO_4$[40,41] and layered $LiCoO_2$.[42]

III. RESULTS AND DISCUSSION

A. LMO bulk

The $LiMn_2O_4$ exhibits a cubic spinel structure at room temperature, which arises from the disordered arrangements of Mn^{3+} and Mn^{4+}. Around 230–280 K the structure undergoes a phase transformation associated with a coupled charge and AF ordering.[43,44] As shown in Table I the crystal structure based on the GGA and GGA + U calculations do not show structure parameters indicative of a cooperative charge ordering and Jahn-Teller distortion unless both a reasonably correct AF ordering and electron localization (GGA + U) are implemented. There are two possible AF arrangements of Mn ions within our supercell of 16 Mn ions: along the (100) and the (110) directions. We adopt the (110) AF ordering, which resembles the spin ordering suggested by the experiments of Tomeno *et al.*[43] insomuch that the Mn ions are arranged in a [↑↑↓↓] pattern along the (110) direction. This is also the lowest energy AF arrangement according to the study of Ouyang *et al.*[19] The bond length for Mn - O was found to be 1.97 Å in the structure with FM ordering, whereas the bond length for Mn–O were 2.02 Å in the structure with AF ordering, highlighting the distortion along the c axis due to the Jahn-Teller effect and in excellent agreement with previous work.[19] The resulting electronic DOS resulting from the relaxed cell exhibits a small band gap of 0.3 eV, in agreement with previous studies using similar parameters.[19]

B. LMO surface stability

The surface energies are calculated by subtracting the energy of the bulk of a specified amount of $LiMn_2O_4$ from the energy of the slab containing the same amount of $LiMn_2O_4$, divided by the surface area of the slab by including both sides. The surface energy, γ, is thus computed as

$$\gamma = \frac{E_{\text{slab}} - N E_{\text{bulk}}}{2A},$$

where E_{slab} is the energy of the slab supercell, E_{bulk} is the bulk energy per atom, N is the number of atoms in the surface slab, and A is the base area of the slab.

The (100), (110), and (111) surfaces of LMO fall in the category of Tasker type III, where it is necessary to redistribute the surface charge by moving some of the surface ions (in our

TABLE II. Calculated surface energies of $LiMn_2O_4$ for the (100), (110), and the (111) low-index directions using GGA + U and GGA (for comparison).

$LiMn_2O_4$ facet	GGA				GGA + U			
	Fixed Volume Slab	Relaxed Volume Slab			Fixed Volume Slab	Relaxed Volume Slab		
	Energy (J/m^2)	Energy (J/m^2)	ΔV%	ΔE%	Energy (J/m^2)	Energy (J/m^2)	ΔV%	ΔE%
Li Terminated (100) (010) (001)	1.24	0.91	19	27	0.96	0.87	10	9.4
Mn/O Terminated (100) (010) (001)	1.50	1.47	8.4	2.0	1.30	1.28	4.7	1.6
Mn/O Terminated (110)	1.50	1.41	7.7	6.0	1.76	1.52	1.1	16
Li/Mn/O Terminated (110)	1.46	1.40	5.6	4.8	1.41	1.39	1.9	1.4
Li/Mn/O Terminated (111)	0.98	0.98	1.8	0.30	1.23	1.18	4.1	5.9
Li Terminated Reconstructed (111)	0.89	0.88	3.2	1.5	0.67	0.65	3.0	1.6

case Li, O, or Mn) from one side of the slab to the other. We calculated the energies of (100), (101), and (111) surfaces of $LiMn_2O_4$ spinel, using the same electronic and magnetic state parameters [GGA + U, AFM(110)], which were optimized to obtain the correct bulk electronic semiconducting state. Although employing GGA is insufficient to capture the correct electronic state of LMO, for comparison, we also used GGA without the $+U$ correction to elucidate the effect on morphology. A summary of the calculated surface energies, in both GGA and GGA + U, are given in Table II and the relaxed surface structures (GGA + U) are shown in Figs. 2–4. In the following text we discuss the results and compare to earlier work.

For the (100) surface we considered both Li-terminated as well as Mn/O-terminated slabs. For the Li-terminated surface we moved one of the two surface Li from the top layer to the bottom one. For the Mn/O-terminated slab, we equalized the amount of O and Mn on the surface layers by moving four O and two Mn from the top to the bottom layer. Beyond thus neutralizing the dipoles, no specific surface reconstruction except that resulting from conventional volume and internal cell parameter structural relaxation was utilized. The calculated surface GGA + U energies were found to be 0.87 (0.96) J/m^2 and 1.28 (1.30) J/m^2 for the Li and Mn/O terminations respectively, where the two values indicate a cell relaxation including the volume (and without). As found by previous work,[20,21] the Li termination is the most stable, which is intuitive as it exhibits less broken bonds/area unit compared to the Mn/O termination. The surface energies vary significantly between the three studies (up to a factor of 3.7), presumably due to differences in cell setup and electronic/magnetic parameters (e.g., Benedek *et al.* employs a FM arrangement for the Mn ions). However, since the resulting particle morphology depends on the *relative* stability of the surfaces we calculate the ratio between the Li-terminated and the Mn/O-terminated $\gamma(\mathrm{Li})/\gamma(\mathrm{Mn/O})$: 1.35 (GGA + U, our work), 1.61 (GGA, our work), 1.4,[20] and 1.68[21] and find the agreement much improved.

The (110) surface was investigated using both Mn/O and Li/Mn/O termination. For the Mn/O termination, we moved two O and one Mn to the bottom layer resulting in two O and one Mn on each surface plane. For the Li/Mn/O termination we equalized the surface charge by moving two O, one Mn, and

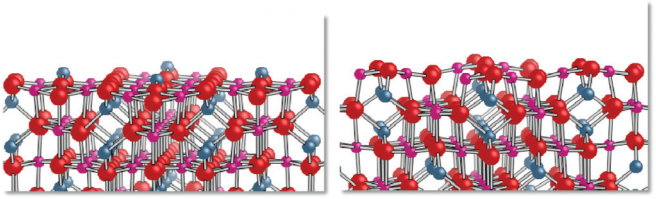

FIG. 2. (Color online) The relaxed (100) surface facet with (a) Li (blue) termination and (b) Mn (magenta)/O (red) termination.

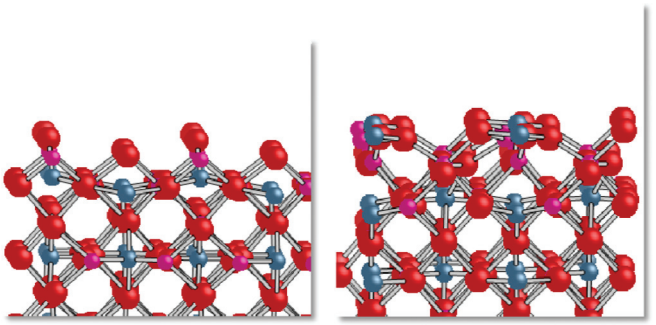

FIG. 3. (Color online) The relaxed (110) surface facet with (a) Mn (magenta)/O (red) termination and (b) Li (blue)/Mn (magneta)/O (red) termination.

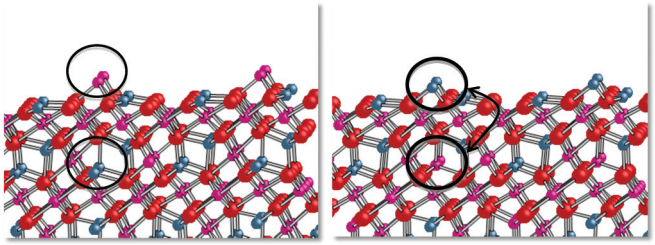

FIG. 4. (Color online) The unreconstructed (111) surface facet with (a) Li (blue)/Mn (magenta)/O (red) termination and (b) the relaxed Li-terminated surface with the inverse spinel surface reconstruction between the undercoordinated surface Mn and bulk fully tetrahedrally coordinated Li as indicated by the circles.

one Li from the top to the bottom layer. Again, only routine cell relaxation was used to arrive at the relaxed surface structure. Similarly, Benedek *et al.*[21] calculated both the Li/Mn/O as well as the Mn/O terminations and found the Li/Mn/O termination to be the lower energy, 0.99 J/m^2, as compared to 1.19 J/m^2. In this work we find the Li/Mn/O terminated GGA + U surface energy to be 1.39 (1.41) J/m^2 for the volume-relaxed (fixed volume) cell and 1.52 (1.76) J/m^2 for the Mn/O terminated surface. Thus, in both studies the Li/Mn/O terminated surface is predicted to be the most stable and, while the absolute surface energies differ between the two works (presumably due to difference in electronic structure parameters), the ratio γ(Mn/O)/γ(Li/Mn/O) is quite similar.

We emphasize that, for both the (100) as well as the (110) LMO surface facets, once the surface dipole has been neutralized, we employ no specific reconstruction of the surface structure beyond the conventional unit cell relaxation.

However, the (111) surface was found by Benedek *et al.*[21] to undergo significant reconstruction, which resulted in extensive migration of O as well as Li from the bulk to the surface layer and distorted square-planar or highly distorted tetrahedrally coordinated Mn ions at the surface. The surface energy of this reconstructed Li/Mn-terminated (111) surface was found to be 0.85 J J/m^2, which was higher than that for their (001) facet (0.58 J/m^2).[21] We believe the significant reconstruction found by Benedek *et al.* to be an indication of the inherent instability of the original (111) surface rather than the final low-energy surface structure, which the MD simulation may have been unable to identify. Indeed, Benedek *et al.*[21] speculate that their reconstructed (111) surface remains in question. To add another piece to the puzzle, x-ray reflectometry (XRR) measurements made on LiMn2O4 films with different orientations showed that the (111) orientation required a more elaborate model, with an additional "impurity" layer, than the other low-index orientations to reproduce the data, alluding to a stronger driving force for reconstruction. To elucidate the final low-energy structure of the (111) LMO surface, we utilize the knowledge derived from previous surface studies that the relative stabilities for a given surface can be attributed to charge and coordination. For example, lower charged surface cations (in this case Li) with a smaller loss in coordination will usually result in more stable surface facets.[45] This was evidenced in Ref. 41 where, for surface facets of $LiFePO_4$, absorbents were most likely to attach themselves to undercoordinated Fe surface ions and in Ref. 42 where undercoordinated Co was found to be energetically very unfavorable compared to undercoordinated Li. To achieve this for the (111) LMO surface we employ a local cation inversion at the surface where we swap the undercoordinated surface Mn ions with Li from the next available layer. This reconstruction leads to a local inverse spinel distribution at the surface where the Li cations occupy the octahedral sites leaving the Mn to occupying the tetrahedral sites. This (111) facet reconstruction has been found to be stable for other spinel systems such as $MgAl_2O_4$.[45] Employing this simple reconstruction scheme, the (111) surface lowers significantly in energy and is found to be the most stable facet among the investigated surfaces at 0.65 J/m^2 (0.67 J/m^2) for the volume-relaxed (non-volume-relaxed) slab, respectively.

In summary, we find that, employing a targeted inverse spinel reconstruction for the (111) surface, the (111) surface has lowest energy among the investigated low-index facets in LMO, in agreement with the experimental findings of Hirayama *et al.*,[3] and indeed most spinel structures.[22] The (100) and the (110) surfaces are less stable but of similar energies to each other.

C. Equilibrium LMO particle shape

The equilibrium LMO particle shape (see Fig. 5) was obtained through the Wulff construction based on the calculated surface energies in Table II, using both GGA + U and GGA for comparison. While the surface energies derived in GGA and GGA + U differ quite substantially by absolute value, the resulting Wulff shape is comparable between the two methodologies due to similar relative surface energies. We do expect the GGA + U results to provide a more accurate rendition of the thermodynamic shape of LMO due to the improved description of the electronic structure for this system. However, in both cases, our calculations show that the (111) surface is the most stable surface facet, which makes the (111) the predominant facet followed by the (100) and (110) surfaces at similar energies. These surface energies result in a cubo-octrahedral particle shape, as seen in Fig. 5, in excellent agreement with previous experimental work[15,16] where $LiMn_2O_4$ particles were found to exhibit a cubo-octahedral shape with predominant (111) facets.

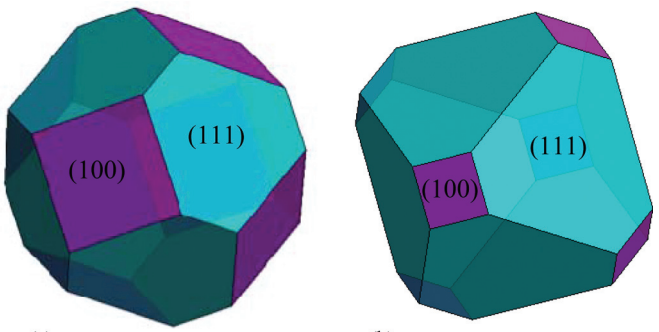

FIG. 5. (Color online) The $LiMn_2O_4$ particle equilibrium cubo-octahedral shape with majority (111) facets (aqua) and minority (100) facets (purple) from the calculated (a) GGA and (b) GGA + U surface energies based on the Wulff construction.

IV. CONCLUSION

In summary, we used first-principles density functional calculations within the GGA + U approximation to calculate the bulk and surface properties of the $LiMn_2O_4$ spinel. Our calculations confirm that a reasonably correct AF ordering along the (110) direction and electron localization (GGA + U) result in a correct semiconducting electronic, Jahn-Teller distorted, and charged-ordered state for the LMO spinel. Using the same electronic parameters we performed calculations of the predominant surface facets (100), (110), and (111). While the (100) and (110) surfaces could be calculated using a conventional cell relaxation procedure, we found that the (111) surface only successfully stabilizes when we site exchange the undercoordinated surface Mn cations with fully coordinated tetrahedral subsurface Li cations, effectively creating a partial inverse spinel arrangement at the surface layer. This selective surface reconstruction lowers the (111) surface energy compared to the (100) and the (010) surface facets and renders the (111) surface the most stable facet in the spinel structure. Comparing to available earlier work, we find that the absolute surface energies vary quite significantly, but the ratios between the energies are similar, except for the (111) surface facet where the employment of a selective ion surface reconstruction significantly lowers this surface energy. In this work, we also determine the equilibrium (Wulff) shape of $LiMn_2O_4$ particle, which exhibits a cubo-octahedral shape with predominant (1 1 1) facets, in good agreement with experimentally found equilibrium shapes of $LiMn_2O_4$ particles.[15,16]

ACKNOWLEDGMENTS

Work at the Lawrence Berkeley National Laboratory was supported by the Assistant Secretary for Energy Efficiency and Renewable Energy, Office of Vehicle Technologies of the US Department of Energy, under Contract No. DEAC02-05CH11231.

[1] H. Yang, S. Amiruddin, H. J. Bang, Y. K. Sun, and J. Prakash, J. Indust. Eng. Chem. **12**, 12 (2006).
[2] M. M. Thackeray, W. I. F. David, P. G. Bruce, and J. B. Goodenough, Mater. Res. Bull. **18**, 461 (1983).
[3] H. W. Chan, J. G. Duh, and S. R. Sheen, J. Power Sources **115**, 110 (2003).
[4] M. Hirayama, H. Ido, K. Kim, and W. Cho, J. Am. Chem. Soc. **14**, 15268 (2010).
[5] M. M. Thackeray, Prog. Solid State Chem. **25**, 1 (1997).
[6] M. M. Thackeray, A. de Kock, M. H. Rossouw, D. Liles, R. Bittihn, and D. Hoge, J. Electrochem. Soc. **139**, 363 (1992).
[7] J. M. Tarascon and D. Guyomard, J. Electrochem. Soc. **138**, 2864 (1991).
[8] R. J. Gummow and M. M. Thackeray, J. Electrochem. Soc. **141**, 1178 (1994).
[9] R. J. Gummow, A. de Kock, and M. M. Thackeray, Solid State Ionics **69**, 59 (1994).
[10] M. M. Thackeray, J. Am. Ceram. Soc. **82**, 3347 (1999).
[11] A. Blyr, C. Sigala, G. G. Amatucci, D. Guyomard, Y. Chabre, and J. M. Tarascon, J. Electrochem. Soc. **145**, 194 (1998).
[12] X. Sun, H. S. Lee, X. Q. Yang, and J. McBreen, Electrochem. Solid-State Lett. **4**, A184 (2001).
[13] Y. Xia, T. Sakai, T. Fujieda, X. Q. Yang, X. Sun, Z. F. Ma, J. McBreen, and M. Yoshio, J. Electrochem. Soc. **148**, A723 (2001).
[14] M. M. Thackeray, Y. Shao-Horn, A. J. Kahaian, K. D. Kepler, E. Skinner, J. T. Vaughey, and S. J. Hackney, Electrochem. Solid-State Lett. **1**, 7 (1998).
[15] H. Huang, C. A. Vincent, and P. G. Bruce, J. Electrochem. Soc. **146**, 3649 (1999).
[16] T. Takada, H. Hayakawa, H. Enoki, E. Akiba, H. Slegr, I. Davidson, and J. Murray, J. Power Sources **81–82**, 505 (1999).
[17] A. Van der Ven, C. Marianetti, D. Morgan, and G. Ceder, Solid State Ionics **135**, 21 (2000).
[18] B. Xu and Y. S. Meng, J. Power Sources **195**, 4971 (2010).
[19] C. Y. Ouyang, S. Q. Shi, and M. S. Lei, J. Alloys Compd. **474**, 370 (2009).
[20] C. Y. Ouyang, X. M. Zeng, Ž Šljivančanin, and A. Baldereschi, J. Chem. Phys. C **114**, 4756 (2010).
[21] R. Benedek and M. M. Thackeray, Phys. Rev. B **83**, 195439 (2011).
[22] W. Tang, X. Yang, Z. Liu, S. Kasaishi, and K. Ooi, J. Mater. Chem. **12**, 2991 (2002).
[23] J.-W. Lee, J.-I. Kim, and S. H. Min, J. Power Sources **196**, 1488 (2011).
[24] W. A. Deer, R. A. Howie, and J. Zussman, *An Introduction to the Rock-Forming Minerals* (Wiley, New York, 1966).
[25] J. P. Perdew, J. A. Chevary, S. H. Vosko, K. A. Jackson, M. R. Pederson, D. J. Singh, and C. Fiolhais, Phys. Rev. B **46**, 6671 (1992).
[26] V. I. Anisimov, J. Zaanen, and O. K. Andersen, Phys. Rev. B **44**, 943 (1991).
[27] V. I. Anisimov, I. V. Solovyev, M. A. Korotin, M. T. Czyżyk, and G. A. Sawatzky, Phys. Rev. B **48**, 16929 (1993).
[28] V. I. Anisimov, F. Aryasetiawan, and A. I. Lichtenstein, J. Phys.: Condens. Matter **9**, 767 (1997).
[29] G. Kresse and D. Joubert, Phys. Rev. B **59**, 1758 (1999).
[30] G. Kresse and J. Hafner, Phys. Rev. B **47**, 558 (1993).
[31] G. Kresse and J. Furthmüler, Comput. Mater. Sci. **6**, 15 (1996).
[32] H. J. Monkhorst and J. D. Pack, Phys. Rev. B **13**, 5188 (1976).
[33] F. Zhou, K. Kang, T. Maxisch, G. Ceder, and D. Morgan, Solid State Commun. **132**, 181 (2004).
[34] G. Trimarchi and N. Binggeli, Phys. Rev. B **71**, 035101 (2005).
[35] D. Kasinathan, J. Kunes, K. Koepernik, C. V. Diaconu, R. L. Martin, I. D. Prodan, G. E. Scuseria, N. Spaldin, L. Petit, T. C. Schulthess, and W. E. Pickett, Phys. Rev. B **74**, 195110 (2006).
[36] W. G. Yin, D. Volja, and W. Ku, Phys. Rev. Lett. **96**, 116405 (2006).
[37] P. W. Tasker, J. Phys. C **12**, 4977 (1979).
[38] J. Goniakowski, F. Finocchi, and C. Noguera, Rep. Prog. Phys. **71**, 016501 (2008).
[39] G. Wulff and Z. Kristallogr, Mineral **34**, 449 (1901).

[40]L. Wang, F. Zhou, Y. S. Meng, and G. Ceder, Phys. Rev. B **76**, 165435 (2007).
[41]K. A. Persson, B. Waldwick, P. Lazic, and G. Ceder, Phys. Rev. B **85**, 235438 (2012).
[42]D. Kramer and G. Ceder, Chem. Mater. **21**, 3799 (2009).
[43]I. Tomeno, Y. Kasuya, and Y. Tsunoda, Phys. Rev. B **64**, 094422 (2001).
[44]M. K. Aydinol, A. F. Kohan, and G. Ceder, J. Power Sources **68**, 664 (1997).
[45]S. C. Parker, P. M. Oliver, N. H. De Leeuw, J. O. Titiloye, and G. W. Watson, Phase Transitions: A Multinational Journal **61**, 83 (1997).
[46]J. Rodriguez-Carvajal, G. Rousse, C. Masquelier, and M. Hervieu, Phys. Rev. Lett. **81**, 4660 (1998).